JOC Featured Article

pubs.acs.org/joc

Mechanistic Studies of Wacker-Type Intramolecular Aerobic Oxidative Amination of Alkenes Catalyzed by $Pd(OAc)_2$/Pyridine

Xuan Ye, Guosheng Liu,† Brian V. Popp, and Shannon S. Stahl*

Department of Chemistry, University of Wisconsin—Madison, 1101 University Avenue, Madison, Wisconsin 53706, United States. †Current address: State Key Laboratory of Organometallics Chemistry, Shanghai Institute of Organic Chemistry, Chinese Academy of Science, 354 Fenglin Road, Shanghai, China, 200032

stahl@chem.wisc.edu

Received November 30, 2010

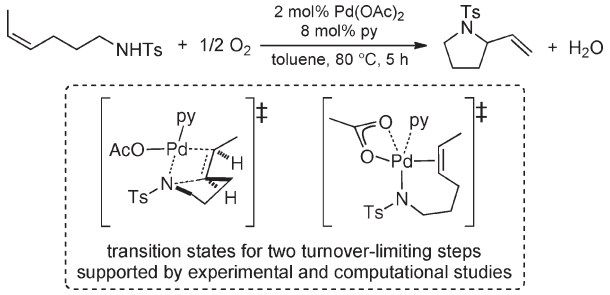

Wacker-type oxidative cyclization reactions have been the subject of extensive research for several decades, but few systematic mechanistic studies of these reactions have been reported. The present study features experimental and DFT computational studies of $Pd(OAc)_2$/pyridine-catalyzed intramolecular aerobic oxidative amination of alkenes. The data support a stepwise catalytic mechanism that consists of (1) steady-state formation of a Pd^{II}-amidate−alkene chelate with release of 1 equiv of pyridine and AcOH from the catalyst center, (2) alkene insertion into a Pd−N bond, (3) reversible β-hydride elimination, (4) irreversible reductive elimination of AcOH, and (5) aerobic oxidation of palladium(0) to regenerate the active *trans*-$Pd(OAc)_2(py)_2$ catalyst. Evidence is obtained for two energetically viable pathways for the key C−N bond-forming step, featuring a pyridine-ligated and a pyridine-dissociated Pd^{II} species. Analysis of natural charges and bond lengths of the alkene-insertion transition state suggest that this reaction is best described as an intramolecular nucleophilic attack of the amidate ligand on the coordinated alkene.

Introduction

Palladium-catalyzed intramolecular aza-Wacker reactions provide access to a number of nitrogen-containing heterocycles such as pyrrolidine, piperazine, oxazolidin-2-one, pyridine, pyrimidyldione and urea deriviatives.[1] These heterocyclization reactions have been a subject of considerable attention, with recent efforts focused especially on the development of new synthetic transformations (e.g., 1,2-difunctionalization of alkenes),[2−6] enantioselective reactions,[7,8] and

(1) Minatti, A.; Muñiz, K. *Chem. Soc. Rev.* **2007**, *36*, 1142–1152.

(2) (a) Ney, J. E.; Wolfe, J. P. *J. Am. Chem. Soc.* **2005**, *127*, 8644–8651. (b) Yip, K.-T.; Yang, M.; Law, K.-L.; Zhu, N.-Y.; Yang, D. *J. Am. Chem. Soc.* **2006**, *128*, 3130–3131. (c) Zeng, W.; Chemler, S. R. *J. Am. Chem. Soc.* **2007**, *129*, 12948–12949. (d) Rosewall, C. F.; Sibbald, P. A.; Liskin, D. V.; Michael, F. E. *J. Am. Chem. Soc.* **2009**, *131*, 9488–9489. (e) Yip, K.-T.; Zhu, N.-Y.; Yang, D. *Org. Lett.* **2009**, *11*, 1911–1914. (f) Sherman, E. S.; Fuller, P. H.; Kasi, D.; Chemler, S. R. *J. Org. Chem.* **2007**, *72*, 3896–3905.

(3) (a) Alexanian, E. J.; Lee, C.; Sorensen, E. J. *J. Am. Chem. Soc.* **2005**, *127*, 7690–7691. (b) Fuller, P. H.; Kim, J.-W.; Chemler, S. R. *J. Am. Chem. Soc.* **2008**, *130*, 17638–17639. (c) Muñiz, K.; Iglesias, A.; Fang, Y. *Chem. Commun.* **2009**, 5591–5593.

(4) (a) Streuff, J.; Hövelmann, C. H.; Nieger, M.; Muñiz, K. *J. Am. Chem. Soc.* **2005**, *127*, 14586–14587. (b) Muñiz, K.; Hövelmann, C. H.; Streuff, J. *J. Am. Chem. Soc.* **2007**, *130*, 763–773. (c) Hövelmann, C. H.; Streuff, J.; Brelot, L.; Muñiz, K. *Chem. Commun.* **2008**, 2334–2336. (d) Sibbald, P. A.; Michael, F. E. *Org. Lett.* **2009**, *11*, 1147–1149.

(5) (a) Helaja, J.; Göttlich, R. *Chem. Commun.* **2002**, 720–721. (b) Manzoni, M. R.; Zabawa, T. P.; Kasi, D.; Chemler, S. R. *Organometallics* **2004**, *23*, 5618–5621. (c) Lei, A.; Lu, X.; Liu, G. *Tetrahedron Lett.* **2004**, *45*, 1785–1788. (d) Michael, F. E.; Sibbald, P. A.; Cochran, B. M. *Org. Lett.* **2008**, *10*, 793–796. (e) Wu, T.; Yin, G.; Liu, G. *J. Am. Chem. Soc.* **2009**, *131*, 16354–16355.

DOI: 10.1021/jo102338a Published on Web 01/20/2011
© 2011 American Chemical Society

methods compatible with the use of molecular oxygen as the terminal oxidant.[9]

Seminal early work by Hegedus[10] and others[11] demonstrated that weakly coordinating nitrogen nucleophiles, especially sulfonamides, are particularly compatible with intramolecular oxidative amination reactions (e.g., eq 1). Early examples of these reactions used benzoquinone or $CuCl_2$ as the stoichiometric oxidant.[10b] Later, the groups of Larock[11d] and Hiemstra[11c] demonstrated that molecular oxygen can be used as an effective oxidant if the reaction is carried out in DMSO as the solvent (eq 2).

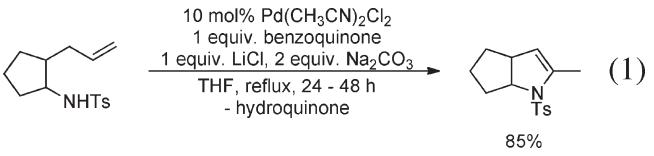

(1)

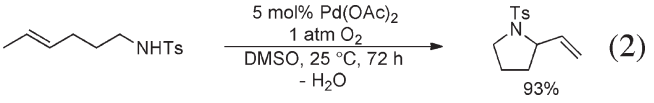

(2)

In 2002, we reported the use of a very simple and efficient $Pd(OAc)_2$/pyridine catalyst system for the intramolecular oxidative amination of alkenes to produce pyrrolidine and pyrroline heterocycles in high yield (Scheme 1).[12,13] This catalyst system, originally reported by Uemura and co-workers for alcohol oxidation,[14] is capable of using molecular oxygen as the stoichiometric oxidant and achieves unprecedented catalytic activity for such reactions. The *p*-toluenesulfonyl (Ts) group proved to be the most effective nitrogen substituent. Substrates bearing the *p*-nitrophenylsulfonyl (Ns) or Cbz ($PhCH_2OC(O)-$) groups were also effective, albeit requiring somewhat longer reaction time. The reaction proceeds well with aromatic and aliphatic tosylamides and tolerates wide variations in solvent polarity, ranging from DMSO to heptane. Nonpolar solvents permit the reaction to be performed at significantly reduced catalyst loading. With 0.2 mol % of $Pd(OAc)_2$ and 0.4 mol % of pyridine in *p*-xylene, the hexenyltosylamide substrate reacted with a turnover rate of 70 h^{-1} during the first 2 h of the reaction, and turnover numbers up to 250−300 were attained. These values are significantly higher than those observed with previous catalyst systems.[10,11] Moreover, this catalyst system has served as the starting point for the development of enantioselective oxidative heterocyclization reactions.[2b,13b,13c]

SCHEME 1. Intramolecular Aerobic Oxidative Amination of Alkenes Catalyzed by $Pd(OAc)_2$/Pyridine[12]

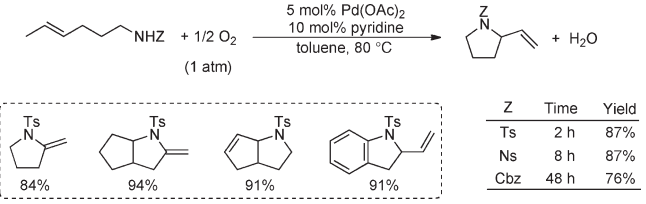

Z	Time	Yield
Ts	2 h	87%
Ns	8 h	87%
Cbz	48 h	76%

Despite the extensive history of Pd-catalyzed oxidative amination reactions, systematic mechanistic investigations have been quite limited. The stereochemical course of the C−N bond-forming step, aminopalladation of alkene, has been a focus of some attention, and evidence for both *cis*-[2a,4b,15] and *trans*-aminopalladation[10a,16] pathways has been obtained (Scheme 2). A recent study from our group demonstrated that the $Pd(OAc)_2$/pyridine-catalyzed intramolecular aerobic oxidative amination reactions (cf. Scheme 1) proceed exclusively via *cis*-aminopalladation of the alkene, consistent with alkene insertion into a palladium−nitrogen bond (Scheme 2).[17] Here, we present experimental and computational studies that provide insight into other important aspects of the catalytic mechanism of $Pd(OAc)_2$/pyridine-catalyzed aerobic oxidative intramolecular amination of alkene. Results include determination of the turnover-limiting step and catalyst resting state, insights into the reversibility of catalytic steps, including those that take place after the turnover-limiting step, and the impact of O_2 pressure on the catalyst stability. These results and their implications for Pd-catalyzed oxidative heterocyclization reactions are presented below.[18]

(6) (a) Tamaru, Y.; Hojo, M.; Yoshida, Z. *J. Org. Chem.* **1988**, *53*, 5731–5741. (b) Harayama, H.; Abe, A.; Sakado, T.; Kimura, M.; Fugami, K.; Tanaka, S.; Tamaru, Y. *J. Org. Chem.* **1997**, *62*, 2113–2122. (c) Shinohara, T.; Arai, M. A.; Wakita, K.; Arai, T.; Sasai, H. *Tetrahedron Lett.* **2003**, *44*, 711–714. (d) Tsujihara, T.; Shinohara, T.; Takenaka, K.; Takizawa, S.; Onitsuka, K.; Hatanaka, M.; Sasai, H. *J. Org. Chem.* **2009**, *74*, 9274–9279.

(7) For a general review on this subject, see: Chemler, S. R. *Org. Biomol. Chem.* **2009**, *7*, 3009–3019.

(8) See refs 2b,2e and 6d and the following: Overman, L. E.; Remarchuk, T. P. *J. Am. Chem. Soc.* **2001**, *124*, 12–13.

(9) For recent reviews describing direct dioxygen-coupled palladium-catalyzed oxidative cyclization reactions, see: (a) Stahl, S. S. *Angew. Chem., Int. Ed.* **2004**, *43*, 3400–3420. (b) Stoltz, B. M. *Chem. Lett.* **2004**, *33*, 362–367. (c) Sigman, M. S.; Schultz, M. J. *Org. Biomol. Chem.* **2004**, *2*, 2551–2554. (d) Stahl, S. S. *Science* **2005**, *309*, 1824–1826. (d) Kotov, V.; Scarborough, C. C.; Stahl, S. S. *Inorg. Chem.* **2007**, *46*, 1910–1923.

(10) (a) Hegedus, L. S.; Allen, G. F.; Waterman, E. L. *J. Am. Chem. Soc.* **1976**, *98*, 2674–2676. (b) Hegedus, L. S.; Allen, G. F.; Bozell, J. J.; Waterman, E. L. *J. Am. Chem. Soc.* **1978**, *100*, 5800–5807. (c) Hegedus, L. S.; Allen, G. F.; Olsen, D. J. *J. Am. Chem. Soc.* **1980**, *102*, 3583–3587. (d) Hegedus, L. S.; McKearin, J. M. *J. Am. Chem. Soc.* **1982**, *104*, 2444–2451.

(11) (a) Tamaru, Y.; Hojo, M.; Higashimura, H.; Yoshida, Z. *J. Am. Chem. Soc.* **1988**, *110*, 3994–4002. (b) Tamaru, Y.; Hojo, M.; Yoshida, Z. *J. Org. Chem.* **1988**, *53*, 5731–5741. (c) van Benthem, R. A. T. M.; Hiemstra, H.; Longarela, G. R.; Speckamp, W. N. *Tetrahedron Lett.* **1994**, *35*, 9281–9284. (d) Larock, R. C.; Hightower, T. R.; Hasvold, L. A.; Peterson, K. P. *J. Org. Chem.* **1996**, *61*, 3584–3585. (e) Harayama, H.; Okuno, H.; Takahashi, Y.; Kimura, M.; Fugami, K.; Tanaka, S.; Tamaru, Y. *Tetrahedron Lett.* **1996**, *37*, 7287–7290. (f) Harayama, H.; Abe, A.; Sakado, T.; Kimura, M.; Fugami, K.; Tanaka, S.; Tamaru, Y. *J. Org. Chem.* **1997**, *62*, 2113–2122. (g) Tamaru, Y.; Kimura, M. *Synlett* **1997**, 749–757.

(12) Fix, S. R.; Brice, J. L.; Stahl, S. S. *Angew. Chem., Int. Ed.* **2002**, *41*, 164–166.

(13) Concurrent with our work, related carbo- and heterocyclization reactions were developed by Stoltz and co-workers: (a) Ferreira, E. M.; Stoltz, B. M. *J. Am. Chem. Soc.* **2003**, *125*, 9578–9579. (b) Trend, R. M.; Ramtohul, Y. K.; Ferreira, E. M.; Stoltz, B. M. *Angew. Chem., Int. Ed.* **2003**, *42*, 2892–2895. (c) Trend, R. M.; Ramtohul, Y. K.; Stoltz, B. M. *J. Am. Chem. Soc.* **2005**, *127*, 17778–17788.

(14) Nishimura, T.; Onoue, T.; Ohe, K.; Uemura, S. *J. Org. Chem.* **1999**, *64*, 6750–6755.

(15) (a) Brice, J. L.; Harang, J. E.; Timokhin, V. I.; Anastasi, N. R.; Stahl, S. S. *J. Am. Chem. Soc.* **2005**, *127*, 2868–2869. (b) Liu, G.; Stahl, S. S. *J. Am. Chem. Soc.* **2006**, *128*, 7179–7181. (c) Isomura, K.; Okada, N.; Saruwatari, M.; Yamasaki, H.; Taniguchi, H. *Chem. Lett.* **1985**, 385–388. (d) Ney, J. E.; Wolfe, J. P. *Angew. Chem., Int. Ed.* **2004**, *43*, 3605–3608. (e) Nakhla, J. S.; Kampf, J. W.; Wolfe, J. P. *J. Am. Chem. Soc.* **2006**, *128*, 2893–2901.

(16) (a) Åkermark, B.; Bäckvall, J. E.; Siirala-Hansén, K.; Sjöberg, K.; Zetterberg, K. *Tetrahedron Lett.* **1974**, *15*, 1363–1366. (b) Åkermark, B.; Bäckvall, J. E.; Hegedus, L. S.; Zetterberg, K.; Siirala-Hansén, K.; Sjöberg, K. *J. Organomet. Chem.* **1974**, *72*, 127–138. (c) Bäckvall, J. E. *Acc. Chem. Res.* **1983**, *16*, 335–342. (d) Bäckvall, J. E.; Björkman, E. E. *Acta Chem. Scand. B* **1984**, *38*, 91–93. (e) Sibbald, P. A.; Rosewall, C. F.; Swartz, R. D.; Michael, F. E. *J. Am. Chem. Soc.* **2009**, *131*, 15945–15951.

(17) Liu, G.; Stahl, S. S. *J. Am. Chem. Soc.* **2007**, *129*, 6328–6335.

SCHEME 2. Possible Pathways for Intramolecular Aminopalladation of Alkenes

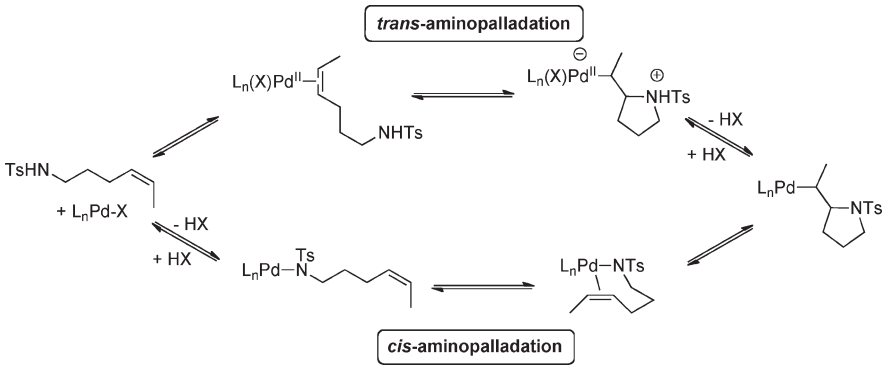

Results and Discussion

Kinetics Studies: Substrate and Catalyst Effects. Intramolecular aerobic oxidative heterocyclization of (*Z*)-4-hexenyltosylamide **1** is catalyzed by $Pd(OAc)_2$/pyridine (2:8 mol %) (eq 3), and the reaction proceeds to completion within 5 h at 80 °C.[19,20] A computer-interfaced gas-uptake apparatus was used to probe the kinetics of the catalytic reaction by monitoring the change in oxygen pressure within a sealed, temperature-controlled reaction vessel. The reaction time-course exhibits a monotonic decrease in pressure (Figure 1), and the lack of an induction period allowed us to obtain much of our kinetic data via initial-rate methods.

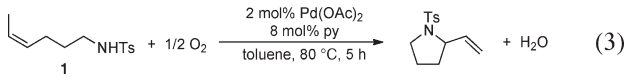

(3)

The initial kinetic studies focused on the influence of the concentration of the primary reaction components (tosylamide, O_2 ,and catalyst) on the initial turnover rate. The data revealed saturation rate dependences on the tosylamide (Figure 2A) and catalyst (Figure 2B) concentrations. The rate dependence on the O_2 pressure was found to be dependent on the $Pd(OAc)_2$/pyridine ratio. At a Pd/py ratio of 1:4, no dependence on O_2 pressure was observed above 300 Torr (Figure 3A). At a Pd/py ratio of 1:2, an apparent O_2 dependence was observed, and the rate observed at the maximum pressure of the reaction vessel was approximately 2-fold higher than the rate observed in the reaction with a 1:4 Pd/py ratio (Figure 3B). In the reaction with Pd/py = 1:2, significant quantities of palladium black were observed at lower O_2 pressures.

Pyridine and Acetic Acid Effect. The initial turnover rates exhibit a sharp dependence on [pyridine] that maximizes at a Pd/py ratio of approximately 1:1−1:1.5 (Figure 4A) and beyond which significant inhibition is observed. A rate dependence on [acetic acid] concentration is also observed. The catalytic turnover rate maximizes at a 1:1 ratio of added acetic acid to $Pd(OAc)_2$ (Figure 4B).

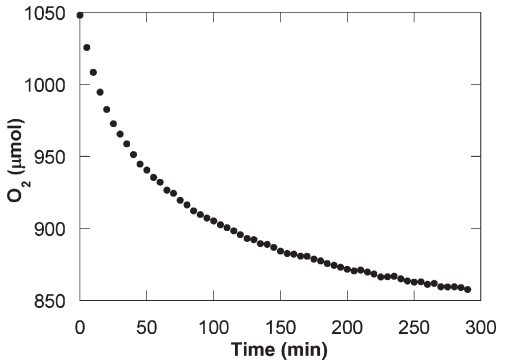

FIGURE 1. Representative kinetic time-course for $Pd(OAc)_2$/pyridine catalyzed intramolecular oxidative amination of (*Z*)-4-hexenyltosylamide obtained by gas-uptake methods. Data sampling occurred at a rate of 1 s^{-1} (not all data are shown). Conditions: $[Pd(OAc)_2]$ = 2.0 mM, [pyridine] = 8.0 mM, [amide] = 100 mM, 4.0 mL of toluene, initial pO_2 = 700 Torr, 80 °C.

If excess pyridine is added to the reaction mixture (120 mM; 10−240 equiv relative to $Pd(OAc)_2$), the initial rate exhibits a square-root dependence on $[Pd(OAc)_2]$ (Figure 5A). This result contrasts the hyperbolic dependence observed when the catalyst concentration is varied at a constant py/Pd ratio of 4:1 (Figure 2B). The rate dependence on $[Pd(OAc)_2]$ changes again if both pyridine and acetic acid are added to the reaction mixture (120 and 5 mM, respectively). Under these conditions, a linear dependence of the rate on $[Pd(OAc)_2]$ is observed (Figure 5B).

Electronic Effects. A series of para-substituted benzenesulfonamides (*p*-X = OMe, H, CH_3, Cl, NO_2) were used to examine electronic effects on the catalytic turnover rate. The Hammett plot (Figure 6) reveals that electron-rich substrates react more rapidly than those bearing electron-withdrawing groups, and a linear fit of the data exhibits a slope (ρ) of −0.22. These results expand upon the qualitative data acquired with the *p*-CH_3 and -NO_2 derivatives (cf. Scheme 1), which showed that the Ns-substituted derivative required a longer reaction time.

(18) For an analogous study of aerobic oxidative amination reactions, catalyzed by an *N*-heterocyclic carbene−Pd^{II} catalyst system, see the following: (a) Rogers, M. M.; Wendlandt, J. E.; Guzei, I. A.; Stahl, S. S. *Org. Lett.* **2006**, *8*, 2257–2260. (b) Ye, X.; Stahl, S. S. Unpublished results.

(19) (*Z*)-4-Hexenyltosylamide was selected instead of (*E*)-4-hexenyltosylamide as the model substrate for this mechanistic study because *cis*-alkenes usually afford better yields in palladium-catalyzed aerobic oxidative amination reactions, possibly due to better coordinating ability of *cis*-alkene to the palladium center.

(20) In our original report of $Pd(OAc)_2$/pyridine-catalyzed intramolecular aerobic oxidative amination of alkenes, a 1:2 ratio of $Pd(OAc)_2$/pyridine was employed. However, in the present study, a 1:4 ratio of $Pd(OAc)_2$/pyridine was used as the standard catalyst mixture because the palladium catalyst is more stable and less susceptible to decomposition in the presence of 4 equiv of pyridine ligand.

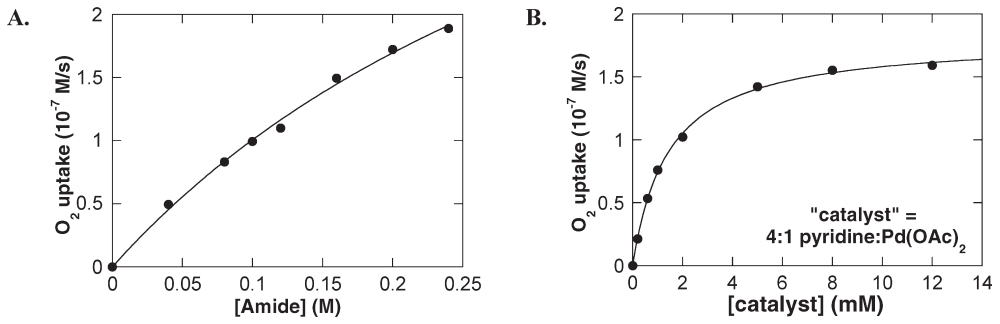

FIGURE 2. (A) Dependence of the initial rate on amide concentration. The curve fit results from a nonlinear least-squares fit to a hyperbolic function of [amide]. Conditions: $[Pd(OAc)_2]$ = 2.0 mM, [pyridine] = 8.0 mM, [amide] = 0−240 mM, 4.0 mL of toluene, initial pO_2 = 700 Torr, 80 °C. (B) Dependence of the initial rate on catalyst concentration, where the "catalyst" is a 4:1 mixture of pyridine and $Pd(OAc)_2$. Conditions: $[Pd(OAc)_2]$ = 0−12.0 mM, [pyridine] = 0−48.0 mM [amide] = 100 mM, 4.0 mL of toluene, initial pO_2 = 700 Torr, 80 °C.

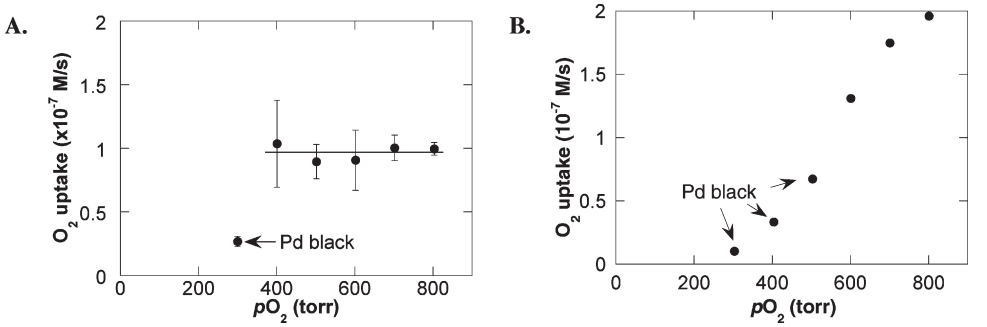

FIGURE 3. (A) Dependence of the initial rate on the initial oxygen pressure (with Pd/py ratio of 1/4). Conditions: $[Pd(OAc)_2]$ = 2.0 mM, [pyridine] = 8.0 mM, [tosylamide] = 100 mM, 4.0 mL of toluene, initial pO_2 = 300−700 Torr, 80 °C. (B) Dependence of the initial rate on the initial oxygen pressure (with Pd/py ratio of 1/2). Conditions: $[Pd(OAc)_2]$ = 2.0 mM, [pyridine] = 4.0 mM, [tosylamide] = 100 mM, 4.0 mL of toluene, initial pO_2 = 300−700 Torr, 80 °C.

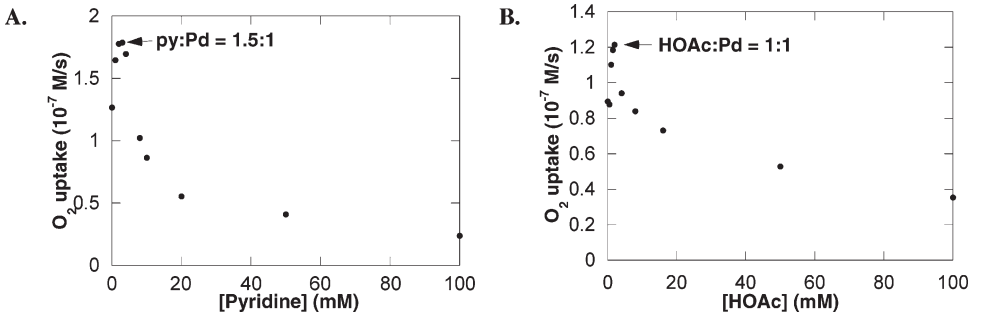

FIGURE 4. (A) Dependence of the initial rate on pyridine concentration with the $[Pd(OAc)_2]$ held constant. Conditions: $[Pd(OAc)_2]$ = 2.0 mM, [pyridine] = 0−10 mM, [amide] = 100 mM, 4.0 mL of toluene, initial pO_2 = 700 Torr, 80 °C. (B) Dependence of the initial rate on acetic acid concentration. Conditions: $[Pd(OAc)_2]$ = 2.0 mM, [pyridine] = 8.0 mM, [amide] = 100 mM, [AcOH] = 0−100 mM, 4.0 mL of toluene, initial pO_2 = 700 Torr, 80 °C.

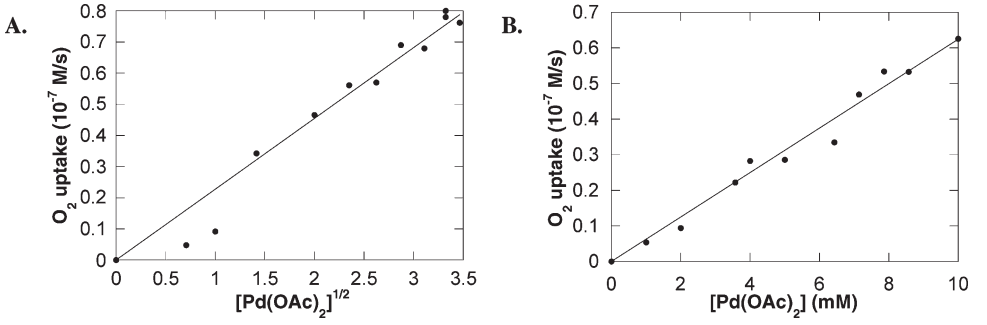

FIGURE 5. (A) Dependence of the initial rate on the square root of $Pd(OAc)_2$ concentration in the presence of a large excess of pyridine. Conditions: [pyridine] = 120 mM, [amide] = 100 mM, 4.0 mL of toluene, initial pO_2 = 700 Torr, 80 °C. (B) Dependence of the initial rate on the concentration of $Pd(OAc)_2$ in the presence of excess pyridine and acetic acid. Conditions: [pyridine] = 120 mM, [AcOH] = 5 mM, [amide] = 100 mM, 4.0 mL of toluene, initial pO_2 = 700 Torr, 80 °C.

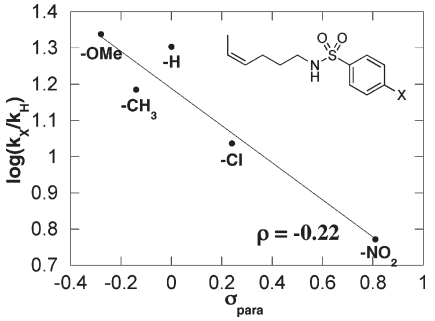

FIGURE 6. Hammett plot derived from the relative initial rates of catalytic oxidative amination conducted with a series of para-substituted benzenesulfonamides. Conditions: $[Pd(OAc)_2]$ = 2.0 mM, [pyridine] = 8.0 mM, [amide] = 100 mM, 4.0 mL of toluene, initial pO_2 = 700 Torr, 80 °C.

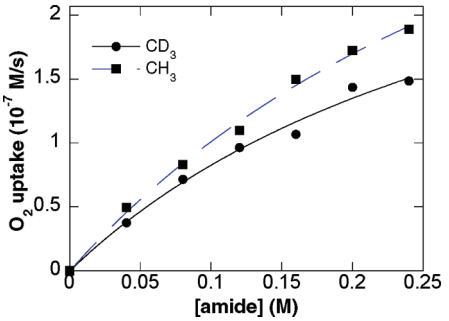

FIGURE 7. Dependence of the initial O_2 uptake rate on amide concentration. CH_3- vs CD_3-labeled tosylamides. Conditions: $[Pd(OAc)_2]$ = 2.0 mM, [pyridine] = 8.0 mM, [amide] = 0−240 mM, 4.0 mL of toluene, initial pO_2 = 700 Torr, 80 °C.

Kinetic Isotope Effects and Isotopic Labeling Studies. Kinetic isotope effects were determined by comparing the independent rates of reaction for tosylamide substrates bearing terminal CH_3- and CD_3- groups (eq 4, Figure 7), as well as NH- vs ND-labeled tosylamides (eq 5, Figure 8). Small, secondary kinetic isotope effects were evident in both cases (1.20 ± 0.05 and 1.15 ± 0.05, respectively).

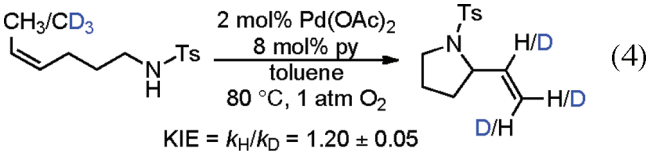

(4)

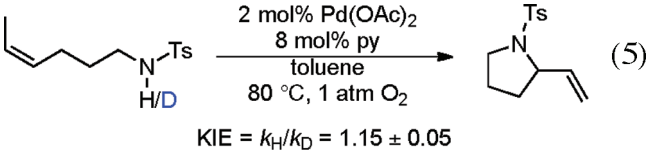

(5)

Deuterium incorporation (~20%) into the β-vinyl position was observed in the reaction of CD_3-labeled tosylamide (eq 4). The scrambling of deuterium label into the internal vinylic position suggests the β-hydride elimination from the palladium−alkyl intermediate is reversible. Crossover

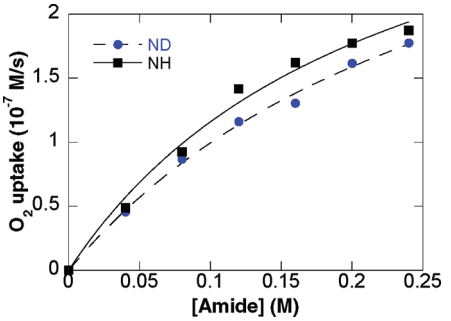

FIGURE 8. Dependence of the initial O_2 uptake rate on amide concentration. NH- vs ND-labeled tosylamides. Conditions: $[Pd(OAc)_2]$ = 2.0 mM, [pyridine] = 8.0 mM, [amide] = 0−240 mM, 4.0 mL of toluene, initial pO_2 = 700 Torr, 80 °C.

experiments demonstrate that this isotopic scrambling takes place exclusively in an intramolecular fashion. No intermolecular deuterium scrambling was observed when the reaction was carried out with a 1:1 mixture of CH_3- and CD_3-labeled tosylamide (eq 6).[21]

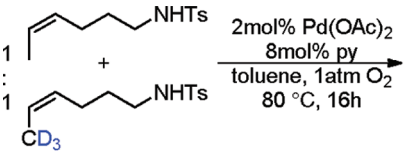

(6)

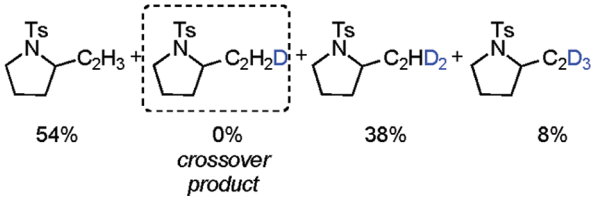

The partially deuterated tosylamide substrates **2** and **3** were utilized to probe the intramolecular kinetic isotope effect associated with β-hydride versus β-deuteride elimination from the palladium−alkyl intermediate **4** (Scheme 3).[22] ^{1}H NMR spectroscopic analysis of final product mixtures reveals an approximately 3:1 distribution between β-hydride elimination and β-deuteride elimination products.

The prospect of reversible aminopalladation was examined with substrate **5**, which features two symmetrical alkenes with isotopically substituted methyl groups (eq 7). Two limiting scenarios are possible with this substrate: (1) if aminopalladation is reversible, the ratio of cyclic products **6** and **7** could approach 3:1, as dictated by the relative rates of β-H versus β-D elimination; (2) if aminopalladation is irreversible, the yield of **6** and **7** should be identical (Scheme 4). When this reaction was performed,

(21) The intramolecular nature of deuterium scrambling into the β-vinyl position of the pyrrolidine product has been independently confirmed by crossover experiment with 1:1 mixture of CD_3-labeled tosylamide and all-protio pyrrolidine products. For a detailed experimental description, see the Supporting Information.

(22) For detailed experimental description, see the Supporting Information.

SCHEME 3. Intramolecular Selectivity between β-Hydride and β-Deuteride Elimination

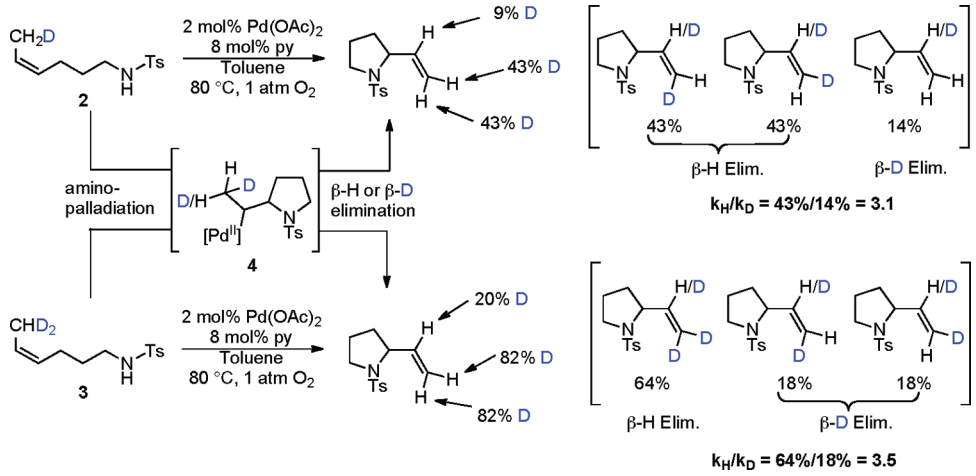

a 1.04:1 ratio of **6**/**7** was obtained, implicating irreversible aminopalladation.

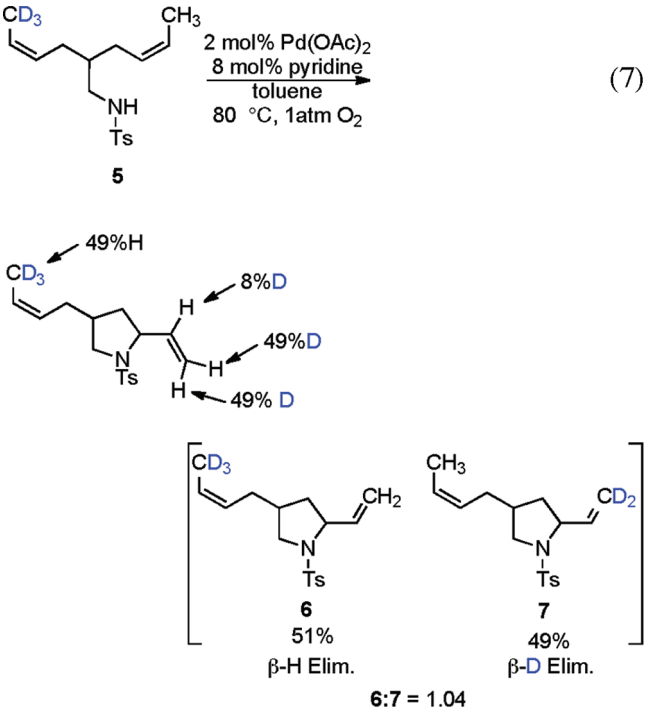

^{1}H NMR Spectroscopic Studies: Characterization of the Catalyst Resting State. ^{1}H NMR spectroscopic studies were conducted to gain insight into the identity of the catalyst resting state. *trans*-$(py)_2Pd(OAc)_2$ forms upon the addition of 2 equiv of pyridine to $Pd(OAc)_2$ and was previously characterized in our mechanistic study of $Pd(OAc)_2$/pyridine-catalyzed aerobic alcohol oxidation.[23] Two sets of pyridine ^{1}H resonances are observed if more then 2 equiv of pyridine are present, corresponding to coordinated and free pyridine. Titration of (*Z*)-4-hexenyltosylamide (from 0 to 77 equiv relative to $Pd(OAc)_2$) into a solution of the catalyst (1:2.2 $Pd(OAc)_2$/py) results in essentially no change of the chemical shifts associated with the coordinated and free pyridine at temperatures ranging from −40 to +40 °C.[22]

SCHEME 4. Probing the Reversibility of Aminopalladation of Alkene with Diene Substrate 5

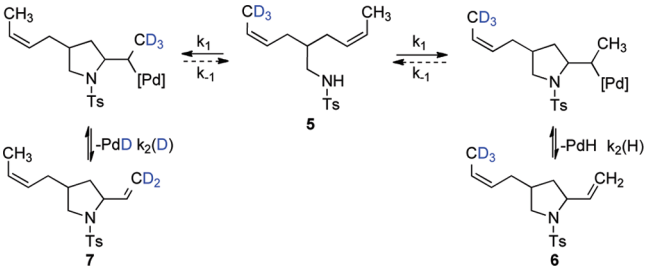

Catalytic Mechanism Based on Experimental Observations. Intramolecular aerobic oxidative amination of alkenes catalyzed by $Pd(OAc)_2$/pyridine proceeds via a Pd^{II}/Pd^0 catalytic cycle in which palladium(II)-mediated substrate oxidation and aerobic oxidation of the catalyst occur in two independent, sequential stages. The kinetic studies described above, which reveal no dependence of the rate on $[O_2]$ and a dependence on [catalyst] and [amide], indicate that a step associated with Pd^{II}-mediated substrate oxidation is turnover-limiting. Consistent with this proposal, *trans*-$(py)_2Pd(OAc)_2$ has been identified as the catalyst resting state, and this species is capable of promoting kinetically competent stoichiometric substrate oxidation in the absence of molecular oxygen.

The catalytic cycle shown in Scheme 5 illustrates a mechanism that is consistent with all of the experimental data presented above. Key features of this mechanism include (1) a two-step sequence for formation of the palladium(II) amidate−alkene chelate **9**, via release of 1 equiv of pyridine and acetic acid (steps i and ii); (2) turnover-limiting alkene insertion into Pd−N bond (step iii); (3) β-hydride elimination from the alkylpalladium(II) intermediate **10** (step iv); and (4) dissociation of product and reductive elimination of AcOH (both included in step v). Reoxidation of a pyridine-ligated Pd^0 species completes the catalytic cycle (step vi).

(23) (a) Steinhoff, B. A.; Stahl, S. S. *Org. Lett.* **2002**, *4*, 4179–4181. (b) Steinhoff, B. A.; Guzei, I. A.; Stahl, S. S. *J. Am. Chem. Soc.* **2004**, *126*, 11268–11278.

SCHEME 5. Proposed Catalytic Mechanism for $Pd(OAc)_2$/Pyridine-Catalyzed Aerobic Oxidative Intramolecular Amination of Alkenes

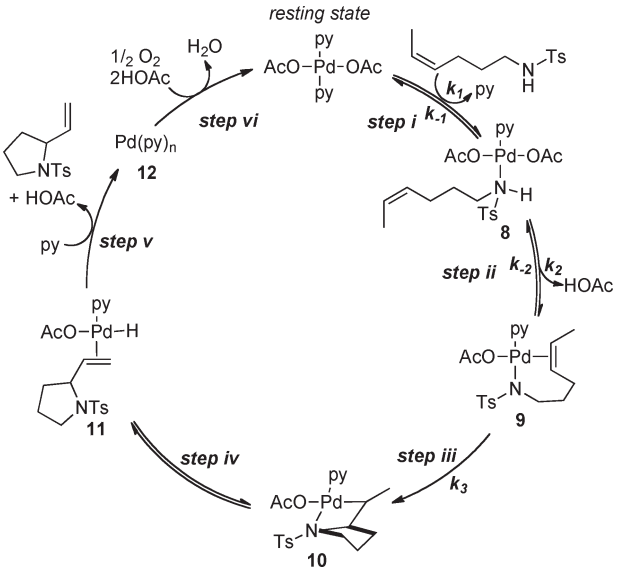

The precise nature and sequence of the first two steps (Scheme 5, steps i and ii) cannot be established from the available data; however, reversible formation of intermediate **9** is consistent with the small N−H/N−D isotope effect (Figure 8), and it rationalizes the inhibitory effect of pyridine and AcOH. The amidate−alkene chelate **9** is the starting point for *cis*-aminopalladation of the alkene.[17]

This mechanism also accounts for the variable [catalyst] dependence observed under different reaction conditions: hyperbolic dependence with a 1:4 Pd/py catalyst system; half-order dependence in the presence of excess pyridine (py/Pd > 10:1); and first-order dependence in the presence of excess pyridine and AcOH (Figure 2B, Figure 5). Nearly identical kinetic behavior was characterized previously for $Pd(OAc)_2$/pyridine-catalyzed alcohol oxidation.[20] These observations are attributed to the kinetic influence of the small pre-equilibrium and/or steady-state quantities of pyridine and AcOH, whose concentrations will be directly proportional to the concentration of the Pd intermediates, **8** and **9**, respectively. If sufficient quantities of pyridine and AcOH are added to ensure that a constant excess concentration of these species is present, a first-order dependence on $[Pd(OAc)_2]$ is observed. A more thorough discussion of this effect has been presented previously,[20] and rate laws, based on steady-state and pre-equilibrium formation of intermediates **8** and **9**, are presented in the Supporting Information.

The neutral ligand, pyridine, plays a key role in the stabilization and aerobic oxidation of palladium(0). At a pyridine/Pd ratio < 4:1 (e.g., 2:1), the catalytic turnover rate exhibits an O_2 dependence and significant palladium-black formation is observed (Figure 3B), indicating a competition between catalyst oxidation and decomposition upon formation of palladium(0). The beneficial rate effect of pyridine, which maximizes at a ~1:1−1:1.5 Pd/pyridine ratio (Figure 4A), probably reflects several factors. Palladium acetate exists as a trimer in nonpolar solvents,[24] and the presence of coordinating ligands lead to the formation of lower nuclearity Pd species that are probably more electrophilic and/or reactive with organic substrates.[25] In addition, pyridine can stabilize the palladium(0) intermediate **12**, either by preventing aggregation or enhancing the reaction rate between **12** and molecular oxygen.[23] At high concentrations, however, pyridine inhibits the catalytic turnover rate because it competes with the substrate for coordination sites at the Pd center.[26]

The addition of excess AcOH strongly inhibits the catalytic turnover rates at high concentrations (Figure 4B). This observation is readily explained by a competition between alkene insertion into the palladium−amidate bond (k_3, Scheme 5) and protonation of palladium amidate intermediate **9** (k_{-2}, Scheme 5). Elevated [AcOH] will favor protonation of **9** and lead to inhibition of catalytic turnover. The origin of the small, but noticeable, beneficial effect of AcOH at low concentrations (Pd/AcOH = 1:1) is less certain but may be related to the ability of AcOH to promote the pyridine-dissociation equilibrium in step i via hydrogen bonding to the pyridine (Figure 4B).[27]

The proposed turnover-limiting alkene insertion into a $Pd-N_{amidate}$ bond (k_3, Scheme 5) is consistent with the observed Hammett correlation (Figure 6). Alkene insertion into the Pd−N bond is expected to be more facile with more-electron-rich (i.e., nucleophilic) amidates.[28] β-Hydride elimination (step iv, Scheme 5) takes place after the turnover-limiting step, and therefore, the proposed mechanism is consistent with the small secondary kinetic isotope effect determined by comparing independent rates of tosylamide substrates bearing terminal CH_3- versus CD_3- groups (Figure 7).

The isotope-labeling studies reveal three key features of the reaction: (1) β-hydride elimination is reversible (cf. eq 4, Scheme 3); (2) deuterium scrambling among the three vinyl positions occurs exclusively in an intramolecular fashion (cf. eq 6); and (3) aminopalladation of alkene is irreversible (cf. Scheme 4). All three observations are accommodated by the proposed mechanism in Scheme 5. Turnover-limiting alkene insertion into the palladium−amidate bond renders the overall aminopalladation of alkene irreversible, and the exclusively intramolecular deuterium scrambling suggests that the product dissociation is irreversible.

(24) Stephenson, T. A.; Morehouse, S. M.; Powell, A. R.; Heffer, J. P.; Wilkinson, G. *J. Chem. Soc.* **1965**, 3632–3640.

(25) In a recent demonstration of this principle, pyridine ligands have been shown to activate Pd-carboxylate catalysts toward C−H activation in the aerobic oxidative coupling of *o*-xylene: Izawa, Y.; Stahl, S. S. *Adv. Synth. Catal.* **2010**, *352*, 3223–3229.

(26) The apparent kinetic dependence on $[O_2]$ when the reaction is carried out in the presence of 1:2 Pd:py (Figure 3B) reflects the fact that at low $[O_2]$ the catalyst decomposes more rapidly, thereby removing active catalyst from the reaction mixture. At higher $[O_2]$, the catalyst is more stable, and the higher concentration of active catalyst contributes to a faster rate. The O_2-pressure effects on catalyst stablility have been analyzed in considerable detail in the following: Steinhoff, B. A.; Stahl, S. S. *J. Am. Chem. Soc.* **2006**, *128*, 4348–4355.

(27) A similar "up/down" dependence on [AcOH] has also been observed by Sigman and co-workers in $Pd(IiPr)(OAc)_2(H_2O)$-catalyzed aerobic alcohol oxidation. In this case, the observation was attributed to a balance between the relative rate of HOAc-inhibited alcohol oxidation and HOAc-promoted palladium catalyst regeneration by O_2. See: Mueller, J. A.; Goller, C. P.; Sigman, M. S. *J. Am. Chem. Soc.* **2004**, *126*, 9724–9734.

(28) For insights into electronic effects on alkene insertion into Pd−N bonds, see: (a) Hanley, P. S.; Markovic, D.; Hartwig, J. F. *J. Am. Chem. Soc.* **2010**, *132*, 6302–6303. (b) Neukom, J. D.; Perch, N. S.; Wolfe, J. P. *J. Am. Chem. Soc.* **2010**, *132*, 6276–6277.

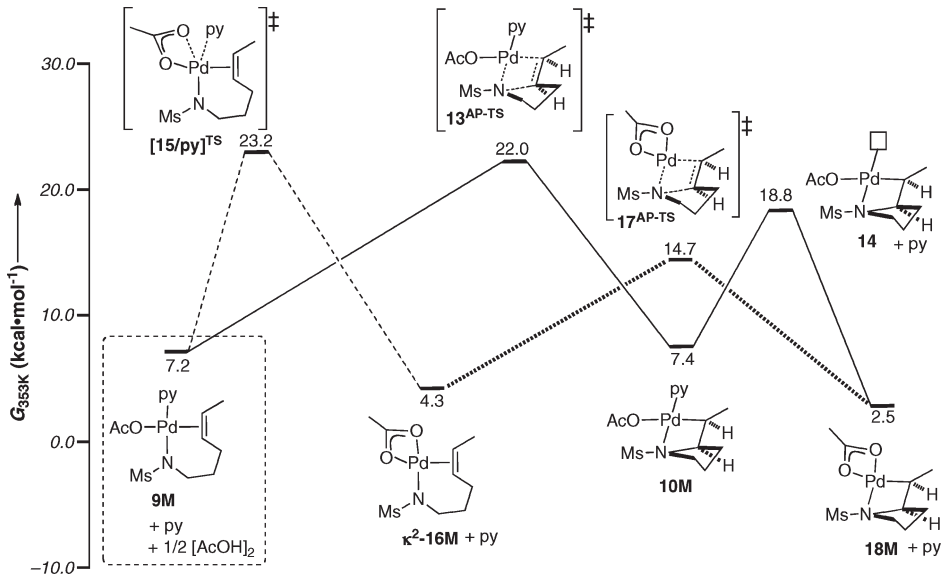

FIGURE 9. Lowest free energy pathways for formation of aminopalladative intermediates with and without pyridine ligation. All reactions are relative to *trans*-(py)$_2$Pd(OAc)$_2$ + **1M**; free py and $^1/_2$[AcOH]$_2$.

Computational Studies. With the mechanistic framework in Scheme 5 as a starting point, we performed computational studies of the oxidative amination mechanism using density functional theory (DFT) methods in order to gain further insights into the energetics of the reaction pathway. These studies employed *trans*-(py)$_2$Pd(OAc)$_2$ as the catalyst with a model substrate, (*Z*)-4-hexenylmesylamide **1M** (eq 8), in which the experimental toluenesulfonyl group was replaced with a methanesulfonyl group in the computational studies (note: for experimental compounds modeled by computed analogues differing only in the identity of the sulfonyl group, we use the experimental compound number with an "M" suffix for the computed structure). The calculations were performed using the B3LYP functional, and the experimental solvent, toluene, was described with a continuum solvent model. Free energies (the only energies discussed here) were calculated for all intermediates and transition states at 80 °C.[29] All calculated free energies presented below are reported relative to the energy of *trans*-(py)$_2$Pd(OAc)$_2$ + **1M**.[30]

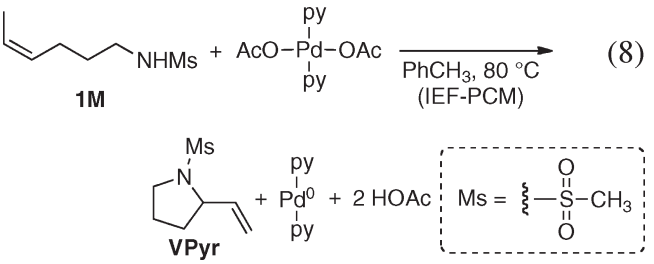

The experimental studies indicate that aminopalladation of the alkene is the turnover-limiting step of the catalytic cycle. The Pd^{II}-amidate−alkene chelate **9M** is the starting point for the aminopalladation step, and the calculated pathway for formation of this species from *trans*-(py)$_2$Pd(OAc)$_2$ + **1M** is presented in the Supporting Information. Two energetically similar pathways were identified for alkene insertion into the palladium−amidate bond, a pyridine-ligated and pyridine-dissociated pathway

SCHEME 6. Calculated Energies for Alternative Aminopalladation Transition States

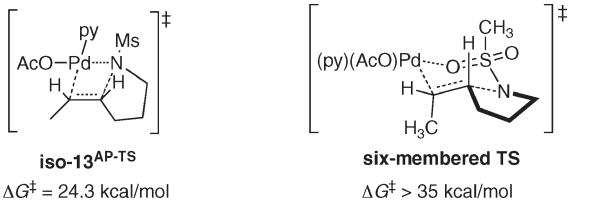

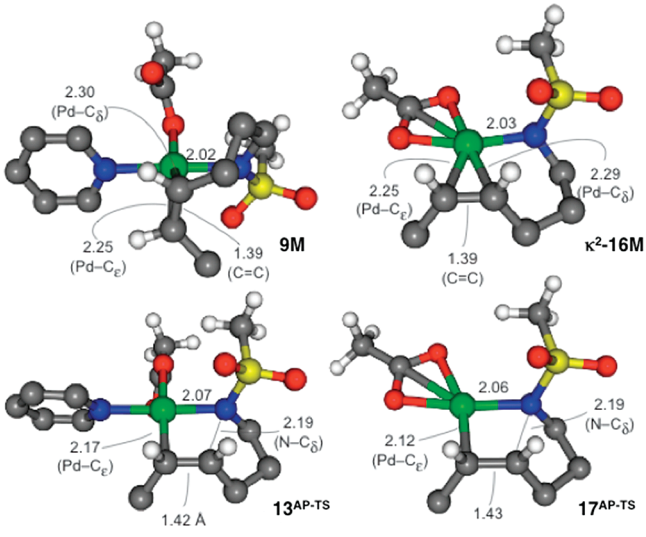

FIGURE 10. Ball-and-stick models with bond-length metrics for the Pd-amidate−alkene intermediates **9M** and **κ^2-16M** and alkene insertion transition states **13^{AP-TS}** and **17^{AP-TS}**.

(29) For further computational details, see the Experimental Section and Supporting Information.

(30) For stuctures lacking pyridine or AcOH, the energies account for the presence of free py and 0.5 equiv of [AcOH]$_2$, respectively.

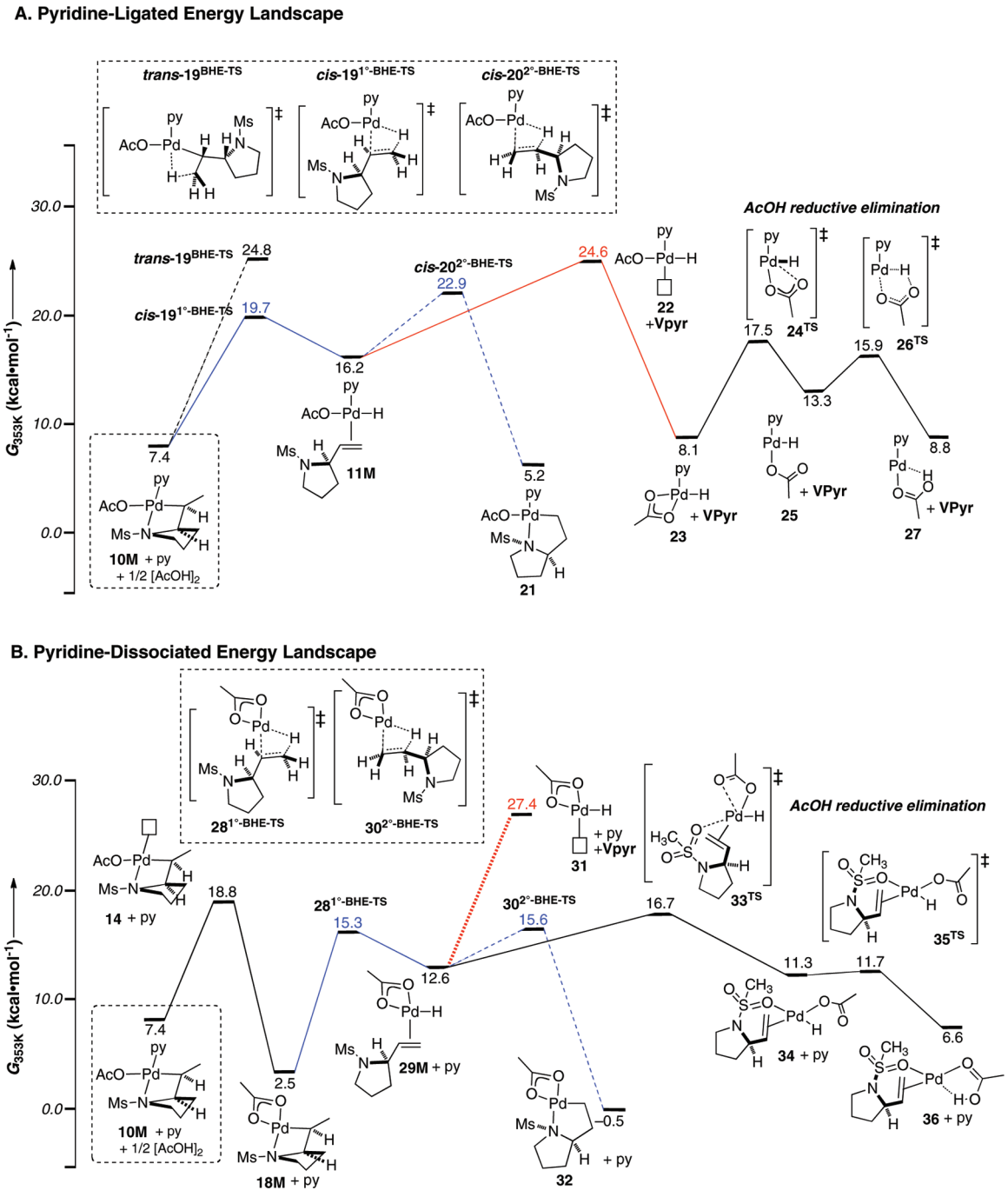

FIGURE 11. Low energy pathways for the β-hydride elimination and AcOH-reductive elimination. All reactions are relative to $(py)_2Pd(OAc)_2$ + **1M**; free py and $^1/_2[AcOH]_2$: (A) pyridine-ligated pathway; (B) pyridine-dissociated pathway.

(Figure 9). The first pathway reflects the proposed mechanism in Scheme 5 and proceeds via transition state $\mathbf{13}^{\mathbf{AP\text{-}TS}}$ for C−N bond formation, in which pyridine is coordinated to the Pd^{II} center (Scheme 5, solid line). Alkene insertion into the Pd−N bond exhibits a barrier of 22.0 kcal/mol. In the other pathway, pyridine dissociates from the Pd center to form a Pd^{II}-amidate−alkene species with a κ^2-acetate ligand, $\boldsymbol{\kappa^2}$**-16M**. Subsequent alkene insertion via the pyridine-dissociated transition state $\mathbf{17}^{\mathbf{AP\text{-}TS}}$ exhibits a much lower barrier, $\Delta G^{\ddagger}$ = 14.7 kcal/mol ($\Delta\Delta G^{\ddagger}$ = −7.3 kcal/mol). In this pathway, pyridine dissociation from Pd^{II} via $[\mathbf{15/py}]^{\mathbf{TS}}$ is calculated to be the rate-limiting step, with a calculated barrier slightly higher (1.2 kcal/mol) than transition state $\mathbf{13}^{\mathbf{AP\text{-}TS}}$. The pyridine-ligated alkyl-Pd^{II} metallacycle **10M** is 4.9 kcal/mol higher in energy than the corresponding pyridine-dissociated species **18M**, which has a κ^2-acetate ligand.

Several other aminopalladation transition states were considered in the course of these studies, but all proved to be higher in energy than those shown in Figure 9. For example, a transition-state isomer of $\mathbf{13}^{\mathbf{AP\text{-}TS}}$, in which the amidate nitrogen atom and alkene are *trans* to acetate and pyridine

ligands, respectively, is 2.3 kcal/mol higher in energy (Scheme 6, *iso*-**13**$^{AP\text{-}TS}$). In addition, pathways that proceed via a six-membered C−N bond-forming transition state, in which a sulfonyl oxygen atom is coordinated to the Pd^{II} center, proved to be much higher in energy (> 35 kcal/mol; see Scheme 6).[29]

The metrical parameters for the Pd-amidate−alkene intermediates **9M** and κ^2-**16M** and the alkene insertion transition states **13**$^{AP\text{-}TS}$ and **17**$^{AP\text{-}TS}$ are shown in Figure 10. The bond lengths together with the calculated natural charges for these species are consistent with a reaction pathway that can be described as an intramolecular nucleophilic attack of the amidate ligand onto a Pd^{II}-activated alkene. For example, transition state **13**$^{AP\text{-}TS}$ features a lengthened carbon−carbon bond relative to **9M** (1.42 vs 1.39 Å, respectively), and the alkene is unsymmetrically coordinated to the palladium center in **13**$^{AP\text{-}TS}$, reflecting a progression toward the 5-*exo*-*trig* cyclization transition-state geometry. Natural charges (NC) on the alkene reflect a highly polarized carbon−carbon bond, NC = −0.38 and +0.07 for the terminal and internal carbon atoms of the alkene, respectively.[29] In addition, the palladium-coordinated nitrogen atom of the sulfonamide has substantial negative charge in **13**$^{AP\text{-}TS}$/NC = −0.86.

The experimental data reveal that β-hydride elimination and subsequent AcOH-reductive-elimination take place after the turnover-limiting step in the catalytic mechanism. Nevertheless, these are important steps in the overall reaction.[31,32] The "pyridine-ligated" intermediate **10M** and the "pyridine-dissociated" intermediate **18M** can both undergo β-hydride elimination, and the energy profiles originating from these species are shown in Figure 11. In both pathways, the energy barriers of vinyl pyrrolidine product dissociation (via structures **22** and **31**; red pathway) are large relative to the barriers associated with isomerization between primary and secondary palladium−alkyl intermediates (blue pathway). Therefore, both pathways are consistent with the experimentally observed intramolecular deuterium scrambling into the β-vinyl position (eq 6). The overall barriers evident on these profiles, however, suggest the "pyridine-ligated" pathway (Figure 11A) is unlikely. The barrier for product dissociation via **22** is calculated to be higher in energy than the barrier calculated for turnover-limiting aminopalladation (Figure 9). Turnover-limiting product dissociation is not consistent with the Hammett correlation observed with the different sulfonamide nucleophiles (Figure 6), and the pyridine-dissociated pathway (Figure 11B) provides an energetically viable alternative for the β-hydride elimination and product dissociation steps.

Modified Proposed Catalytic Mechanism. The collection of experimental and computational data presented above provides the basis for a slightly revised catalytic cycle for the Pd(OAc)$_2$/pyridine-catalyzed aerobic oxidative intramolecular amination of alkenes (Scheme 7). This mechanism reflects the two possible aminopalladation pathways, in which the Pd^{II}-amidate−alkene intermediate **9** can react via a pyridine-ligated pathway or a pyridine-dissociated pathway. The former pathway features direct insertion of the alkene into the palladium−amidate bond (Scheme 7, **9** → **10**), followed by dissociation of the pyridine from Pd^{II} (**10** → **18**). The latter pathway features dissociation of pyridine prior to the insertion of alkene into the palladium-amidate bond (Scheme 7, **9** → **16** → **18**). The two proposed pathways feature different turnover limiting steps, alkene insertion (**9** → **10**) vs pyridine disscociation (**9** → **16**), both of which are consistent with the experimental data, including (a) the rate law, (b) the Hammett plot (pyridine dissociation should proceed more rapidly with more-electron-rich *trans* amidate ligands), and (c) reversible β-hydride elimination *after* the turnover-limiting step of the mechanism.

SCHEME 7. Refined Catalytic Mechanism for Pd(OAc)$_2$/Pyridine-Catalyzed Aerobic Oxidative Intramolecular Amination of Alkenes

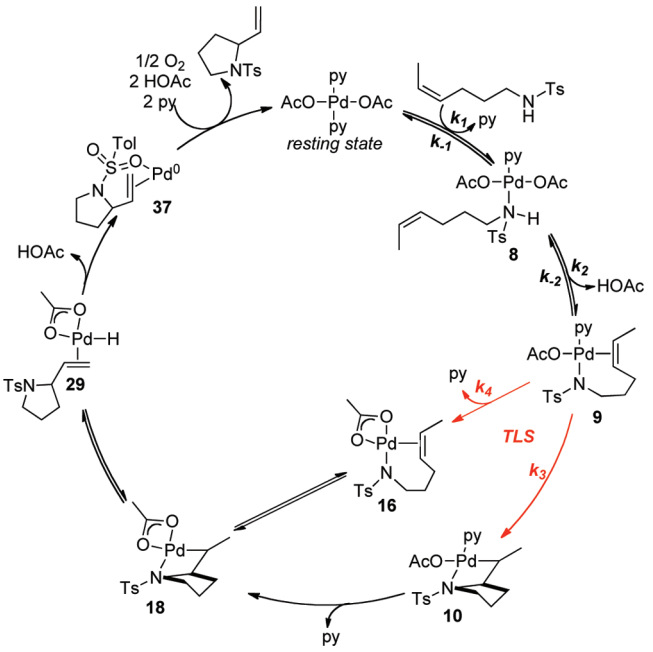

The pyridine-dissociated pathway for β-hydride elimination (Scheme 7, **18** → **29**) is favored over the originally proposed pyridine-ligated pathway (Scheme 5, **10** → **11**) based on computational analysis. The regeneration of palladium(II) catalyst from palladium-hydride intermediate **29** proceeds via irreversible reductive elimination of AcOH. Facile reoxidation of palladium(0) complex **37** takes place in competition with catalyst decomposition.

Conclusion

The mechanistic study presented in this paper provides a thorough analysis of palladium-catalyzed Wacker-type aerobic oxidative amination reactions. Experimental and computational data suggest a catalytic mechanism that consists of (1) steady-state formation of a Pd^{II}-amidate−alkene intermediate, (2) alkene insertion into a Pd−N bond, (3) reversible β-hydride elimination, (4) irreversible AcOH reductive elimination, and (5) aerobic oxidation of palladium(0) to regenerate the active catalyst *trans*-Pd(OAc)$_2$(py)$_2$. Two energetically viable pathways, including a pyridine-ligated

(31) Although pathways involving direct reaction of a Pd−H species with molecular oxygen have been proposed to initiate catalyst regeneration, recent computational work provides compelling evidence that this catalytic system must proceed through Pd^0; see: (a) Popp, B. V.; Stahl, S. S. *Chem.—Eur. J.* **2009**, *15*, 2915–2922. (b) Keith, J. M.; Goddard, W. A. *J. Am. Chem. Soc.* **2009**, *131*, 1416–1425.

(32) For a thorough description of β-hydride elimination and HOAc-reductive elimination pathways, see the Supporting Information.

and a pyridine-dissociated pathway, have been identified for the key C−N bond-forming step. The difference between these two nearly isoenergetic pathways lies in the coordination environment at Pd when the alkene inserts into the palladium−amidate bond. Analysis of natural charges and bond lengths of the alkene-insertion transition state reveal that this formal migratory insertion process can be described as an intramolecular attack of the nitrogen nucleophile onto the coordinated alkene. The possible involvement of ligand-dissociated pathways for nucleopalladation of alkenes has important practical implications for the development of enantioselective reactions. Dissociation of a chiral ligand from Pd^{II} will result in formation of an achiral catalyst. Depending on the relative energies of the other steps in the mechanism, this process could account for some of the historical difficulty in developing enantioselective Wacker-type oxidative cyclization reactions.

Experimental Section

Representative Procedure for Gas-Uptake Kinetics. A typical reaction was conducted as follows. A 25 mL round-bottom flask with a stirbar was attached to an apparatus with a calibrated volume and a pressure transducer designed to measure the gas pressure within the sealed reaction vessel. The apparatus was evacuated to 10 Torr and filled with oxygen to 800 Torr, and this cycle was repeated 10 times. The pressure was established at 675 Torr. When the pressure stabilized in the apparatus, stock solutions of $Pd(OAc)_2$ (2.5 mM, in 3.2 mL toluene) and pyridine (1.2M, in 0.4 mL toluene) were added via syringe through a septum. The flask was heated to 80 °C. When the temperature stabilized, stock solution of substrate (1.0 M, in 0.4 mL toluene) was added via syringe through a septum. Data was acquired using custom software written within LabVIEW. Correlations between oxygen uptake and conversion were made by analysis by ^{1}H NMR spectroscopy with 1,3,5-trimethoxybenzene as an internal standard.

Representative Procedure for Reactions with Isotopically Labeled Substrates. $Pd(OAc)_2$ (0.4 mg, 2 μmol) was added to 13 × 100 mm disposable culture tubes. The reaction tubes were placed into a custom 48-well parallel reactor mounted on a large capacity mixer, and the headspace was purged with molecular oxygen for ca. 15 min. Solutions of pyridine (8 μmol in 0.5 mL of toluene) and substrate (0.1 mmol in 0.5 mL of toluene) were added to the tubes. The reactions were carried out for 24 h under an oxygen atmosphere (1 atm) at 80 °C. Following removal of the solvent under vacuum, the crude oxidative amination product was purified via column chromatography with ethyl acetate/hexanes and analyzed by ^{1}H NMR spectroscopy.

Substrate Syntheses. (*Z*)-4-Hexenylbenzenesulfonamide 1.

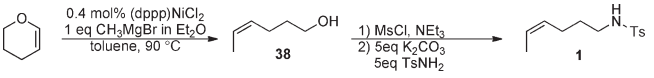

cis-4-Hexen-1-ol **38** was prepared by a modification of the literature procedure.[33] A 3.0 M ethereal solution of MeMgBr (100 mL, 0.3 mmol) was added to a stirring suspension of $(dppp)NiCl_2$ (610 mg, 1.1 mmol) in 200 mL of dry toluene under an N_2 atmosphere. The stirring was continued at room temperature for 20 min. 4,5-Dihydropyran (25 g, 0.3 mol) was added, and the solution was heated to 90 °C and stirred overnight. The cooled reaction mixture was poured into a saturated ammonium chloride solution and extracted with ether. The extract was dried with $MgSO_4$, and the solvent was removed under vacuum. The residue was purified by distillation to afford *cis*-4-hexen-1-ol (27 g, 90% yield). The identity and purity of *cis*-4-hexen-1-ol was confirmed by comparison of the ^{1}H NMR spectrum to that reported in the literature.[33]

(*Z*)-4-Hexenyltoluenesulfonamide **1** was prepared via sequential formation of the mesylate from *cis*-4-hexen-1-ol and S_N2 substitition of the mesylate by tosylamide according to literature procedures.[17]

(*Z*)-4-Hexenyltoluenesulfonamide-d_3 (6-d_3-1).

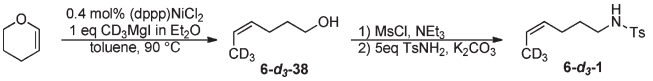

The procedure for preparation of CD_3-labeled (*Z*)-4-hexenyltoluenesulfonamide **6-d_3-1** was the same as that of (*Z*)-4-hexenyltoluenesulfonamide, with the exception that CD_3MgI (1.0 M in diethyl ether) was used instead of CH_3MgBr.[33] (*Z*)-4-Hexenylbenzenesulfonamide-d_3: ^{1}H NMR ($CDCl_3$) δ 7.74 (dt, J = 8.4, 1.8 Hz, 2H), 7.31 (dt, J = 8.4, 1.8 Hz, 2H), 5.44 (dt, J = 10.8, 0.9 Hz, 1H), 5.27 (dt, J = 7.2, 10.8 Hz, 1H), 4.50 (t, J = 6.0 Hz, 1H), 2.95 (dt, J = 6.9, 6.3 Hz, 2H), 2.43 (s, 3H), 2.03 (dq, J = 7.2, 1.2 Hz, 2H), 1.54 (m, 2H); ^{2}H NMR ($CHCl_3$) δ 1.52 (s, 3D); ^{13}C NMR ($CDCl_3$) δ 143.5, 137.2, 129.9, 129.2, 127.3, 125.2, 43.1, 29.5, 24.1, 21.7, 12.1 (heptad, J = 19.2 Hz); HRMS (ESI) calcd for $C_{13}H_{16}D_3NO_2SNa$ 279.1223, found 279.1211.

CH_2D-labeled (*Z*)-4-hexenyltosylamide 2.

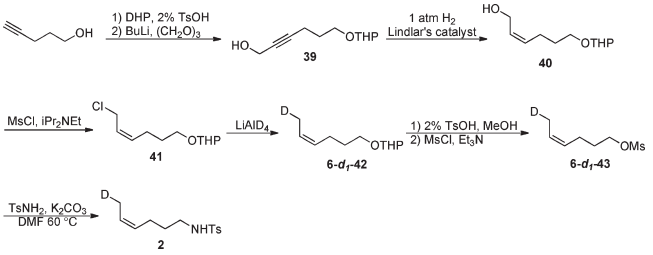

40. Alkyne **39** was synthesized according to literature procedures.[34] To a solution of **39** (4 g, 20 mmol) in MeOH (50 mL) were added Lindlar's catalyst (100 mg) and quinoline (1 mL, 8.5 mmol). The mixture was agitated under an H_2 atmosphere (8 psig) at room temperature for 2 h. The catalyst was filtered, and the solvent was removed under vacuum. The residue was purified by silica gel chromatography (hexane/ethyl acetate) to afford **40** (3.23 g, 79% yield over three steps): ^{1}H NMR ($CDCl_3$) δ 5.66 (m, 1H), 5.50 (m, 1H), 4.53 (dd, J = 4.2, 2.7 Hz, 1H), 4.24 (ddd, J = 12.6, 7.2, 1.2 Hz, 1H), 4.10 (ddd, J = 12.6, 7.2, 1.2 Hz, 1H), 3.86 (m, 1H), 3.74 (dt, J = 9.6, 6.6 Hz, 1H), 3.48 (M, 1H), 3.39 (dt, J = 9.6, 6.6 Hz, 1H), 3.12 (br, 1H), 2.20 (m, 2H), 1.81−1.50 (m, 8H).

41. To a solution of allylic alcohol **40** (3 g, 15 mmol) in methylene dichloride (50 mL) were added ^{i}Pr$_2$NEt (2.6 g, 20 mmol) and MsCl (1.8 g, 16 mmol) at 0 °C via syringe. The reaction was monitored by TLC. After the reaction was complete, water (40 mL) was added. The mixture was extracted with diethyl ether. The extract was dried with $MgSO_4$, and the solvent was removed under vacuum. The residue was purified by silica gel chromatography (hexane/ethyl acetate) to afford **41** (1.9 g, 59% yield): ^{1}H NMR ($CDCl_3$) δ 5.66 (m, 2H), 4.57 (dd, J = 4.2, 2.7 Hz, 1H), 4.16 (d, J = 5.1 Hz, 2H), 3.88 (m, 1H), 3.75 (dt, J = 9.6, 6.6 Hz, 1H), 3.50 (m, 1H), 3.39 (dt, J = 9.6, 6.6 Hz, 1H), 2.23 (m, 2H), 1.71−1.50 (m, 8H).

(33) Wenkert, E.; Michelotti, E. L.; Swindell, C. S.; Tingoli, M. *J. Org. Chem.* **1984**, *49*, 4894–4899.

(34) Heitz, M. P.; Wagner, A.; Mioskowski, C.; Noel, J. P.; Beaucourt, J. P. *J. Org. Chem.* **1989**, *54*, 500–503.

6-d_1-42. Under an N_2 atmosphere, $LiAlD_4$ (150 mg, 4 mmol) was suspended in dry diethyl ether (20 mL). Compound **41** (600 mg, 2.8 mmol) was added slowly via a syringe to this solution. The resulting suspension was refluxed for 2 h. Excess $LiAlD_4$ was quenched with water and then with an aqueous solution of NaOH (40%, 10 mL). The mixture was stirred for 1 h. The white solid was filtered, and the solvent was removed under vacuum to afford crude **6-d_1-42** (471 mg, 91%): ^{1}H NMR ($CDCl_3$) δ 5.44 (m, 2H), 4.58 (dd, J = 4.2, 2.7 Hz, 1H), 3.87 (m, 1H), 3.75 (dt, J = 9.6, 6.6 Hz, 1H), 3.50 (M, 1H), 3.39 (dt, J = 9.6, 6.6 Hz, 1H), 2.12 (m, 2H), 1.71−1.50 (m, 10H).

6-d_1-43. To a solution of crude **6-d_1-42** (471 mg, ~2.6 mmol) in MeOH (5 mL) was added $TsOH\cdot H_2O$ (10 mg, 0.05 mmol). The mixture was stirred for 1 h. Then Na_2CO_3 (50 mg, 0.5 mmol) was added, and the mixture was stirred for 30 min. The solid was filtered, and the solvent was removed under low vacuum. The crude oil was dissolved in CH_2Cl_2 (20 mL), and Et_3N (1 mL) and MsCl (400 mg, 3.5 mmol) were then added slowly via syringe. The mixture was stirred overnight at room temperature. After the reaction was complete (by TLC), water (20 mL) was added. The mixture was extracted with diethyl ether. The extract was dried with $MgSO_4$, and the solvent was removed under vacuum. The residue was purified by silica gel chromatography (hexane/ethyl acetate) to afford **6-d_1-43** (214 mg, 78% yield): ^{1}H NMR ($CDCl_3$) δ 5.52 (m, 1H), 5.37 (m, 1H), 4.23 (t, J = 6.6 Hz, 2H), 3.01 (s, 3H), 2.18 (q, J = 7.2 Hz, 2H), 1.83 (m, 2H), 1.60 (m, 2H); ^{13}C NMR ($CDCl_3$) δ 128.4, 125.9, 69.7, 37.5, 29.1, 22.8, 12.7 (t, J = 19.6 Hz).

2. This compound was prepared according to the literature procedure used for **1**[17] (60% yield, colorless oil): ^{1}H NMR ($CDCl_3$) δ 7.76 (dt, J = 8.4, 1.8 Hz, 2H), 7.31 (dt, J = 8.4, 1.8 Hz, 2H), 5.45 (m, 1H), 5.28 (m, 1H), 4.42 (t, J = 1.8 Hz, 1H), 2.95 (dt, J = 6.9, 6.3 Hz, 2H), 2.43 (s, 3H), 2.03 (q, J = 7.2 Hz, 2H), 1.54 (m, 4H); ^{2}H NMR ($CHCl_3$) δ 1.53 (s, 1D); ^{13}C NMR ($CDCl_3$) δ 143.6, 137.3, 129.9, 129.1, 127.4, 125.4, 43.1, 29.6, 24.2, 21.7, 12.9 (t, J = 19.8 Hz); HRMS (ESI) calcd for $C_{13}H_{18}DNO_2S$, 254.1199, found 254.1192.

CHD_2-Labeled (*Z*)-4-Hexenyltosylamide 3.

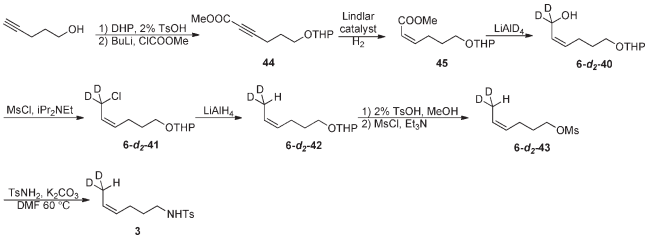

45. The compound **44** was synthesized from 4-pentyn-1-ol according to literature procedures.[35] Compound **44** was hydrogenated according to the procedure used for compound **40** to afford **45** (95%, colorless oil): ^{1}H NMR ($CDCl_3$) δ 6.28 (dt, J = 11.7, 7.5 Hz, 1H), 5.79 (dt, J = 11.7, 1.8 Hz, 1H), 4.58 (dd, J = 4.2, 2.7 Hz, 1H), 3.88 (m, 1H), 3.75 (dt, J = 9.6, 6.6 Hz, 1H), 3.70 (s, 3H), 3.50 (m, 1H), 3.41 (dt, J = 9.6, 6.6 Hz, 1H), 2.75 (m, 2H), 1.81−1.45 (m, 8H).

6-d_2-40. Under an N_2 atmosphere, $LiAlD_4$ (1.1 g, 27 mmol) was suspended in dry diethyl ether (40 mL). Compound **45** (3.4 g, 15 mmol) was added to this suspension at −20 °C via syringe. The mixture was warmed to 0 °C and stirred for 2 h. The excess $LiAlD_4$ was quenched with water, and then an aqueous solution of NaOH (40%, 10 mL) was added. The mixture was stirred for 1 h. The white solid was filtered, and the solvent was removed under vacuum to afford crude **6-d_2-40** (2.8 g, 93%): ^{1}H NMR ($CDCl_3$) 5.70 (d, J = 10.8 Hz, 1H), 5.50 (ddd, J = 10.8, 8.4, 6.6 Hz, 1H), 4.52 (dd, J = 4.2, 2.7 Hz, 1H), 3.86 (m, 1H), 3.75 (dt, J = 9.6, 6.6 Hz, 1H), 3.49 (m, 1H), 3.41 (dt, J = 9.6, 6.6 Hz, 1H), 2.30 (m, 2H), 2.19 (s, 1H), 1.79−1.51 (m, 8H).

6-d_2-41. This compound was prepared according to the procedure used for **41** (see above) (62% yield): ^{1}H NMR ($CDCl_3$) δ 5.41 (m, 2H), 4.58 (dd, J = 4.2, 2.7 Hz, 1H), 3.88 (m, 1H), 3.75 (dt, J = 9.6, 6.6 Hz, 1H), 3.50 (m, 1H), 3.39 (dt, J = 9.6, 6.6 Hz, 1H), 2.13 (m, 2H), 1.71−1.50 (m, 8H).

6-d_2-42. Under an N_2 atmosphere, $LiAlH_4$ (500 mg, 13 mmol) was suspended in dry diethyl ether (40 mL). Then **6-d_2-41** (1.5 g, 6.8 mmol) was added via a syringe. The mixture solution was refluxed for 2 h. The excess $LiAlH_4$ was quenched by water, and then an aqueous solution of NaOH (40%, 10 mL) was added. The mixture was stirred for 1 h. The white solid was filtred, and the solvent was removed under vacuum to afford crude **6-d_2-42** (1.18 g, 94%): ^{1}H NMR ($CDCl_3$) δ 5.65 (m, 2H), 4.57 (dd, J = 4.2, 2.7 Hz, 1H), 3.86 (m, 1H), 3.76 (dt, J = 9.6, 6.6 Hz, 1H), 3.52 (m, 1H), 3.39 (dt, J = 9.6, 6.6 Hz, 1H), 2.23 (m, 2H), 1.71−1.50 (m, 9H).

6-d_2-43. This compound was synthesized according to the procedure used for **6-d_1-43** (see above) (75% yield over two steps): ^{1}H NMR ($CDCl_3$) δ 5.57 (m, 1H), 5.39 (m, 1H), 4.27 (t, J = 6.6 Hz, 2H), 3.06 (s, 3H), 2.21 (q, J = 7.2 Hz, 2H), 1.86 (m, 2H), 1.63 (m, 1H); ^{13}C NMR ($CDCl_3$) δ 128.5, 125.9, 69.7, 37.6, 29.1, 22.9, 12.4 (p, J = 19.6 Hz).

3. Compound **3** was prepared according to the literature procedure used for **1**[17] (60% yield, colorless oil): ^{1}H NMR ($CDCl_3$) δ 7.76 (dt, J = 8.4, 1.8 Hz, 2H), 7.30 (dt, J = 8.4, 1.8 Hz, 2H), 5.45 (dd, J = 10.8, 6.6 Hz, 1H), 5.27 (m, 1H), 4.52 (t, J = 1.8 Hz, 1H), 2.96 (dt, J = 6.9, 6.6 Hz, 2H), 2.43 (s, 3H), 2.03 (q, J = 7.2 Hz, 2H), 1.54 (m, 3H); ^{2}H NMR ($CDCl_3$) δ 1.51 (s, 2D); ^{13}C NMR ($CDCl_3$) δ 143.6, 137.3, 129.9, 129.1, 127.3, 125.3, 43.1, 29.6, 24.2, 21.7, 12.4 (t, J = 19.6 Hz); HRMS (ESI) calcd for $C_{13}H_{17}D_2NO_2S$ 255.1262, found 255.1259.

Diene 5.

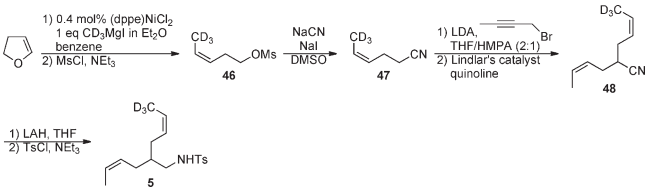

46. The compound was prepared by a modification of the literature procedure.[36] A 1.0 M ethereal solution of CD_3MgI (35 mL, 35 mmol) was added to a stirring suspension of $(dppe)NiCl_2$ (526 mg, 1 mmol) in 40 mL of dry benzene under N_2, and stirring was continued at room temperature for 20 min. 4,5-Dihydropyran (2.8 g, 40 mmol) was added, and the solution was refluxed for 2 h. The cooled reaction mixture was poured into a solution of saturated ammonium chloride and extracted with ether. The extract was dried with $MgSO_4$, and the solvent was removed under reduced pressure. The crude product was dissolved in toluene, and Et_3N (6 mL) and MsCl (0.44 mL, 4.5 mmol) were added slowly via syringe to the toluene solution. The mixture was stirred overnight at room temperature. After the reaction was completed, water (20 mL) was added. The mixture was extracted with diethyl ether. The extract was dried with $MgSO_4$ followed by the removal of solvent under reduced pressure. The residue was purified by silica gel chromatography (hexane/ethyl acetate) to afford **46** (5.4 g, 92% yield over two steps): ^{1}H NMR ($CDCl_3$) δ 5.64

(35) Kita, Y.; Okunaka, R.; Honda, T.; Shindo, M.; Taniguchi, M.; Kondo, M.; Sasho, M. *J. Org. Chem.* **1991**, *56*, 119–125.

(36) Wadman, S.; Whitby, R.; Yeates, C.; Kocienski, P.; Cooper, K. *J. Chem. Soc., Chem. Commun.* **1987**, 241–243.

(d, J = 10.8 Hz, 1H), 5.38 (dt, J = 10.8, 7.2 Hz, 1H), 4.22 (t, J = 6.9 Hz, 2H), 3.00 (s, 3H), 2.51 (dq, J = 6.9, 1.5 Hz, 2H).

47. To a solution of **46** (5.4 g, 3.2 mmol) in DMSO (20 mL), NaCN (1.6 g, 3.2 mmol), and NaI (480 mg, 3.2 mmol) were added under an N_2 atmosphere. The mixture was stirred at 55 °C for 12 h. After the reaction was complete, water (50 mL) was added. The mixture was extracted with diethyl ether. The extract was dried with $MgSO_4$, and the solvent was removed under vacuum. The residue was purified by distillation to give **47** (2.8 g, 89% yield, colorless liquid): ^{1}H NMR ($CDCl_3$) δ 5.64 (d, J = 10.8 Hz, 1H), 5.41 (m, 1H), 2.40 (m, 4H).

48. The compound was prepared by a modification of the literature procedure.[37] To a solution of **47** (1.1 g, 11 mmol) in a 2:1 (volume ratio) mixture of THF and HMPA was slowly added via syringe a solution of LDA (6.1 mL 1.8 M in THF, 11 mmol) at −78 °C under an N_2 atmosphere. After the solution was stirred for 30 min at −78 °C, 1-bromo-2-butyne (1.6 g, 15 mmol) was added.[38] The mixture was stirred for 3 h at −78 °C and then was warmed to room temperature. After the reaction was complete, water (40 mL) was added. The mixture was extracted with diethyl ether. The extract was dried with $MgSO_4$, and the solvent was removed under vacuum. The residue was purified by silica gel chromatography (hexane/ethyl acetate) to give **48** (750 mg, 45% yield over two steps): ^{1}H NMR ($CDCl_3$) δ 5.69 (m, 2H), 5.44 (m, 2H), 2.58 (p, J = 7.2 Hz, 1H), 2.39 (m, 4H), 1.66 (dp, J = 6.9, 0.9 Hz, 3H); ^{13}C NMR ($CDCl_3$) δ 128.4, 128.2, 125.1, 125.0, 122.1, 32.0, 29.13, 29.11, 13.2; HRMS (ESI) calcd for $C_{10}H_{12}D_3NNa$ 175.1290, found 175.1295.

5. Under an N_2 atmosphere, **48** (350 mg, 2.3 mmol) was added to a suspension of $LiAlH_4$ (150 mg, 4 mmol) in dry THF (10 mL) at 0 °C, and the mixture was stirred overnight at room temperature. After the reaction was complete, water (0.5 mL) was added. To the crude reaction mixture Et_3N (1 mL) and TsCl (570 mg, 3 mmol) were added via a syringe. The mixture was stirred for 12 h. After the reaction was complete, water (20 mL) was added. The mixture was extracted with diethyl ether. The extract was dried with $MgSO_4$, and the solvent was removed under vacuum. The residue was purified by silica gel chromatography (ethyl acetate/hexanes) to afford **5** (550 mg, 77% yield, colorless oil): ^{1}H NMR ($CDCl_3$) δ 7.74 (dt, J = 8.4, 1.8 Hz, 2H), 7.31 (dt, J = 8.4, 1.8 Hz, 2H), 5.51 (m, 2H), 5.29 (m, 2H), 4.54 (t, J = 1.8 Hz, 1H), 2.87 (t, J = 6.6 Hz, 2H), 2.43 (s, 3H), 2.01 (t, J = 6.9 Hz, 4H), 1.60 (m, 1H), 1.55 (dt, J = 6.9, 0.9 Hz, 3H); ^{2}H NMR ($CHCl_3$) δ 1.49 (s, 3D); ^{13}C NMR ($CDCl_3$) δ 143.5, 137.2, 129.9, 127.9, 127.8, 127.3, 126.3, 126.2, 46.9, 39.1, 29.43, 29.41, 21.7, 13.1; HRMS (ESI) calcd for $C_{17}H_{22}D_3NO_2SNa$ 333.1692, found 333.1705.

Computational Studies. All computations were performed with the Gaussian 03 (G03) program[39] using resources provided by NSF TeraGrid partners. Spin-restricted density functional theory (RDFT)[40] calculations were performed with the hybrid density-functional, B3LYP.[41,42] A combination of the Stuttgart RSC 1997 ECP[43] for Pd and the all-electron 6-31+G(d) basis sets (Basis I)[44] for all other atoms were used for gas-phase geometry optimization and normal-mode analyses. Full geometry optimizations were carried out in internal coordinates using the Berny algorithm.[45] Frequency calculations were performed at optimized geometries and transition states, confirming that each optimized minimum has zero imaginary frequencies and each optimized transition state has exactly one imaginary frequency. When visual inspection of the single negative eigenvalue defining a saddle point did not clearly confirm the reaction trajectory, IRC calculations were performed to verify that the identified transition state corresponded to the appropriate reactant/product potential energy surface.[46] Zero-point energy and additional thermochemical corrections were calculated at 80 °C using the identified normal modes. Charge analyses were carried out on converged spin-restricted density matrices using the natural population analysis (NPA) method[47] as implemented within NBO 3.1 in G03.

At the calculated stationary points, solvation-corrected single-point total energy calculations were carried out with the Pd basis detailed above and the 6-311+G(d,p) basis (Basis II) on all other atoms with electrostatic and nonelectrostatic solvation effects evaluated using the integral-equation-formalism polarizable-continuum model (IEF-PCM).[48] These calculations were used to predict the solvation free energy under typical catalytic conditions (i.e., toluene solvent at 80 °C (353 K)). The solvation cavity was generated using UFF radii, explicitly treating hydrogen atoms, and the radii were scaled by a factor of 1.2. The PCM input was modified with the following parameters to define the physical characteristics of the solvent (ε = 2.24, ρ = 0.810 g·cm^{-1}, r = 2.82 Å). The dielectric constant (ε) used here was determined with eq 9.[49] The temperature range over which eq 9 is reported is 207−316 K; however, we find that eq 9 reproduces, with necessary accuracy, dielectric constants at the higher temperature examined here.[50] The density (ρ) of toluene at 353 K was determined using a 24-parameter empirical model

(37) Petschen, I.; Parrilla, A.; Bosch, M. P.; Amela, C.; Botar, A. A.; Camps, F.; Guerrero, A. *Chem.—Eur. J.* **1999**, *5*, 3299–3309.

(38) Kurth, M. J.; Decker, O. H. W. *J. Org. Chem.* **1985**, *50*, 5769–5775.

(39) Gaussian 03, Revision D.01: Frisch, M. J.; Trucks, G. W.; Schlegel, H. B.; Scuseria, G. E.; Robb, M. A.; Cheeseman, J. R.; Montgomery, J. A., Jr.; Vreven, T.; Kudin, K. N.; Burant, J. C.; Millam, J. M.; Iyengar, S. S.; Tomasi, J.; Barone, V.; Mennucci, B.; Cossi, M.; Scalmani, G.; Rega, N.; Petersson, G. A.; Nakatsuji, H.; Hada, M.; Ehara, M.; Toyota, K.; Fukuda, R.; Hasegawa, J.; Ishida, M.; Nakajima, T.; Honda, Y.; Kitao, O.; Nakai, H.; Klene, M.; Li, X.; Knox, J. E.; Hratchian, H. P.; Cross, J. B.; Bakken, V.; Adamo, C.; Jaramillo, J.; Gomperts, R.; Stratmann, R. E.; Yazyev, O.; Austin, A. J.; Cammi, R.; Pomelli, C.; Ochterski, J. W.; Ayala, P. Y.; Morokuma, K.; Voth, G. A.; Salvador, P.; Dannenberg, J. J.; Zakrzewski, V. G.; Dapprich, S.; Daniels, A. D.; Strain, M. C.; Farkas, O.; Malick, D. K.; Rabuck, A. D.; Raghavachari, K.; Foresman, J. B.; Ortiz, J. V.; Cui, Q.; Baboul, A. G.; Clifford, S.; Cioslowski, J.; Stefanov, B. B.; Liu, G.; Liashenko, A.; Piskorz, P.; Komaromi, I.; Martin, R. L.; Fox, D. J.; Keith, T.; Al-Laham, M. A.; Peng, C. Y.; Nanayakkara, A.; Challacombe, M.; Gill, P. M. W.; Johnson, B.; Chen, W.; Wong, M. W.; Gonzalez, C.; Pople, J. A. Gaussian, Inc.: Wallingford, CT, 2004.

(40) Koch, W., Holthausen, M. C. *A Chemist's Guide to Density Functional Theory*; Wiley-VCH: Weinheim, 2000.

(41) Becke, A. D. *J. Chem. Phys.* **1993**, *98*, 1372–1377.

(42) Lee, C.; Yang, W.; Parr, R. G. *Phys. Rev. B* **1988**, *37*, 785–789.

(43) (a) The Stuttgart RSC 1997 ECP basis set for Pd was obtained from the Extensible Computational Chemistry Environment Basis Set Database, version 02/25/04, as developed and distributed by the Molecular Science Computing Facility, Environmental and Molecular Sciences Laboratory, which is part of the Pacific Northwest Laboratory, P.O. Box 999, Richland, WA 99352, and funded by the U.S. Department of Energy. The Pacific Northwest Laboratory is a multiprogram laboratory operated by Battelle Memorial Institute for the U.S. Department of Energy under contract DE-AC06-76RLO 1830. (b) Andrae, D.; Häussermann, U.; Dolg, M.; Stoll, H.; Preuss, H. *Theor. Chim. Acta* **1990**, *77*, 123–141.

(44) Hehre, W. J.; Radom, L.; Schleyer, L. P. v. R.; Pople, J. A. *Ab Initio Molecular Orbital Theory*; Wiley: New York, 1986.

(45) (a) Peng, C. Y.; Ayala, P. Y.; Schlegel, H. B.; Frisch, M. J. *J. Comput. Chem.* **1996**, *17*, 49–56. (b) Peng, C. Y.; Schlegel, H. B. *Isr. J. Chem.* **1993**, *33*, 449–454.

(46) (a) Gonzalez, C.; Schlegel, H. B. *J. Chem. Phys.* **1989**, *90*, 2154–2161. (b) Gonzalez, C.; Schlegel, H. B. *J. Chem. Phys.* **1990**, *94*, 5523–5527.

(47) Reed, A. E.; Weinstock, R. B.; Weinhold, F. *J. Chem. Phys.* **1985**, *83*, 735–746.

(48) For an overview of solvation models and reviews on PCM methods, see: (a) Tomasi, J.; Mennucci, B.; Cammi, R. *Chem. Rev.* **2005**, *105*, 2999–3093. (b) Cramer, C. J.; Truhlar, D. G. *Chem. Rev.* **1999**, *99*, 2161–2200. For references on our current approach, see: (c) Cancès, E.; Mennucci, B.; Tomasi, J. *J. Chem. Phys.* **1997**, *107*, 3032–3041. (d) Mennucci, B.; Tomasi, J. *J. Chem. Phys.* **1997**, *106*, 5151–5158. (e) Mennucci, B.; Cancès, E.; Tomasi, J. *J. Phys. Chem. B* **1997**, *101*, 10506–10517. (f) Tomasi, J.; Mennucci, B.; Cancès, E. *THEOCHEM* **1999**, *464*, 211–226.

(49) Lide, D. R. *Handbook of Chemistry and Physics*, 88th ed.; CRC Press: Boca Raton, 2007.

(50) Kandil, M. E.; Marsh, K. N.; Goodwin, A. R. H. *J. Chem. Eng. Data* **2008**, *53*, 1056–1065.

that is valid for $T = 223-423$ K and $P = 1-30$ atm.[51]

$$\varepsilon(T) = 3.26 - 0.00344T + 1.59 \times 10^{-6}T^2 \quad (9)$$

We report Gibbs free energies at 353 K (ΔG_{353K}) (eqs 10−13). Since the reported free energies are corrected for a solvated environment, an additional energy correction (S_{corr}) to the translation entropy component of the gas-phase entropy was included. This correction (eq 13) is necessary to account for the standard state change from gas (1 atm) to solution (1 M).[52]

$$E_{solv} = E_{tot} + G_{sol} \quad (10)$$

$$H_{353K} = E_{sol} + \sum_i \frac{1}{2}h\nu_i + \sum_i \frac{h\nu_i}{e^{h\nu_i/k_b T} - 1} + \frac{n}{2}k_b T \quad (11)$$

where n = the number of rotational and translational modes

$$G_{353K} = H_{353K} - T(S_{353K} + S_{corr}) \quad (12)$$

$$S_{corr} = RT(Q^\circ/Q) = 2.36\ \text{kcal}\cdot\text{mol}^{-1} \quad (13)$$

where $R = 0.001987\ \text{kcal}\cdot\text{mol}^{-1}\cdot\text{K}^{-1}$ and $T = 353.15$ K and $Q^\circ/Q = 28.977$.

Acknowledgment. We are grateful to the NIH for financial support of this work (R01 GM67163) and the NSF for partial support of the computational studies through Teragrid resources provided by NCSA and the Pittsburgh Supercomputing Center (TG-CHE070040N).

Supporting Information Available: Experimental details, characterization for all new compounds, and computational data. This material is available free of charge via the Internet at http://pubs.acs.org.

(51) McLinden, M. O.; Splett, J. D. *J. Res. Natl. Inst. Stand. Technol.* **2008**, *113*, 29–67.

(52) Cramer, C. J. *Essentials of Computational Chemistry: Theories and Models*; Wiley: New York, 2002; pp 341−342.